

33

Linear and Multivalent PEGylation of Tobacco Mosaic Virus and the 1 **Effects on its Biological Properties** 2 3 Reca Marian Caballero¹, Ivonne González-Gamboa², Stephen L. Craig³, Nicole F. Steinmetz^{1,2,4,5,6,7,8*} 4 5 Department of Bioengineering, University of California, San Diego, La Jolla, CA, USA 6 ²Department of NanoEngineering, University of California, San Diego, La Jolla, CA, USA 7 ³Department of Chemistry, Duke University, Durham, North Carolina 27708, USA 8 ⁴Department of Radiology, University of California, San Diego, La Jolla, CA, USA 9 ⁵Moores Cancer Center, University of California, San Diego, La Jolla, CA, USA 10 ⁶Institute for Materials Discovery and Design, University of California, San Diego, La Jolla, CA, 11 **USA** 12 ⁷Center for Nano-Immuno Engineering, University of California, San Diego, La Jolla, CA, USA 13 ⁸Center for Engineering in Cancer, University of California, San Diego, La Jolla, CA, USA 14 * Correspondence: 15 Corresponding Author 16 nsteinmetz@ucsd.edu 17 18 Keywords: plant virus, tobacco mosaic virus, PEGylation, cell uptake, immune evasion, protein 19 corona 20 21 22 **Abstract** 23 Plant virus-based nanoparticles (VNPs) offer a bio-inspired approach to the delivery of drugs and 24 imaging agents. The chemical addressability, biocompatibility, and scalable manufacturability make 25 VNPs a promising alternative to synthetic delivery platforms. However, proteinaceous VNPs and synthetic nanoparticles (NPs) alike are readily recognized and cleared by the immune system and 26 27 mechanisms such as opsonization and phagocytosis. Shielding strategies such as PEGylation are 28 commonly used to mitigate premature NP clearance. Here, we investigated polyethylene glycol 29 (PEG) coatings on tobacco mosaic virus (TMV), which was used as a model nanocarrier system. Specifically, we evaluated the effects of linear and multivalent PEG coatings at varying chain lengths 30 31 on serum protein adsorption, antibody recognition, and macrophage uptake. Linear and multivalent

PEGs of MW 2000 and 5000 Da were successfully grafted onto TMV at ~20-40% conjugation

efficiencies, and the degree of crosslinking as a function of PEG arm valency and length was

- outlined. PEGylation resulted in the modulation of TMV-macrophage interactions and reduced
- corona formation as well as antibody recognition. Linear and multivalent PEG 5000 formulations
- 36 (but not PEG 2000) reduced α-TMV antibody recognition, while shorter, multivalent PEG coatings
- significantly reduced α -PEG recognition this highlights an interesting interplay between the NP
- and PEG itself in potential antigenicity and should be an important consideration in PEGylation
- 39 strategies. This work provides insight in PEGylation strategies of VNPs which may improve their
- 40 possibility of implementation in clinical applications.

42 1 Introduction

- Nanoparticles (NPs) are emerging as promising tools in drug delivery and diagnostic applications,
- 44 overcoming limitations of small molecule therapeutics or contrast agents. Free drug molecules or
- 45 contrast agents are limited by their passive diffusion through circulation, giving rise to off-target
- 46 adverse side effects and limiting the achievement of efficacious drug dosages (1). NPs help overcome
- 47 these limitations by facilitating delivery to selective cell types, improving cargo stability and
- solubility, and prolonging circulation times, thus enhancing the efficacy and safety of free drugs (2).
- 49 NPs have been designed to carry and deliver large payloads of small molecules (3–5), proteins (6,7)
- including antigens (8,9), and imaging agents (10,11) in a variety of indications including but not
- 51 limited to diabetes (6,12), cancer (13–15), and Alzheimer disease (16). The co-attachment of
- 52 targeting agents onto NPs is currently being explored to enhance cell and tissue-specific delivery
- 53 (17–19).
- Though there are promising NPs in the development pipeline, systemically delivered NPs must
- overcome biological barriers to successfully deliver their payloads to their target site. The
- mononuclear phagocytic system (MPS) composes of monocytes, tissue-resident macrophages,
- 57 granulocytes, and dendritic cells and serves as a critical immune defense mechanism to NP delivery
- in which exogenous materials are rapidly cleared, processed, and degraded (20). Other challenges
- 59 include opsonization of NPs by antibodies and complement proteins which facilitates phagocytosis
- by cells in the MPS (20). Serum proteins in biological fluids also rapidly interact with NPs and form
- a protein corona around its surface, promoting non-specific uptake of NPs by cells (21). Thus,
- 62 efficacious shielding methods must be utilized to evade such biological barriers for improved
- 63 systemic delivery.
- One major approach to particle shielding is coating the surface of NPs or other therapeutic agents
- with polyethylene glycol (PEG), termed as PEGylation. PEGylation has been demonstrated to impart
- 66 'stealth' properties such as increasing systemic circulation time, decreasing serum protein adsorption,
- and reducing interactions with cells of the MPS (22–24). The shielding ability of PEG arises from its
- 68 molecular and physical properties. PEG, an inert and exceedingly hydrophilic polymer, forms a
- 69 hydration shell with a large, excluded volume that sterically hinders blood components from
- 70 interacting with the NP core (25) Furthermore, the high flexibility and mobility of PEG chains
- 71 grafted onto the surface of NPs renders interactions between the NP and circulating
- biomacromolecules thermodynamically unfavorable (25). The success of PEGylation has led to over
- 73 10 FDA-approved PEGylated drugs to date, of these includes PEGylated nanoparticle medicines such
- as Janssen's liposomal doxorubicin (Doxil) for various cancers and Merrimack's liposomal
- 75 irinotecan (Onivyde) for metastatic pancreatic cancer (26,27). A wide variety of PEGs with
- 76 molecular weights ranging from <1 to 40 kDa in linear or branched conformations have been
- implemented in the list of FDA-approved PEGylated drugs (26). Lipomedix's PEGylated liposomal
- 78 mitomycin-C for solid tumors and Enceladus' PEGylated liposomal prednisolone for rheumatoid

- arthritis are currently undergoing clinical trials attesting to the ongoing pipeline of intravenous
- 80 PEGylated nanoparticles (27).
- In this work, we examined tobacco mosaic virus (TMV), a plant virus nanoparticle (VNP), as a
- 82 nanocarrier platform. TMV and other VNPs pose many advantages due to their biological nature.
- VNPs are highly monodisperse, inexpensively produced at the milligram-gram scale, and non-
- 84 infectious to humans. Their high degree of stability, biocompatibility, and biodegradability make
- VNPs an attractive alternative to synthetic nanotechnologies. Specifically, TMV is a rigid, rod-
- shaped plant virus measuring 300 nm in length and 18 nm in width and consists of 2130 identical
- coat proteins that self-assemble around a single-stranded, positive-sense RNA molecule. A key
- 88 feature of TMV is its high aspect ratio and its anisotropic shape which confers different advantages
- 89 over spherical counterparts. Rod-shaped and filamentous structures have been demonstrated to impart
- 90 tumor homing properties by enhanced margination to vessel walls and increased penetration into
- 91 tumor tissues compared to nanospheres (28). High aspect ratio nanoparticles also present prolonged
- 92 circulation times because their shape better evades macrophages (29,30). Anisotropic nanocarriers
- provide a higher surface area to increase drug loading and delivery while also improving cell binding
- and target cell interactions (31). However, manufacturing high aspect ratio particles precisely and
- 95 consistently at the nanoscale is technically demanding when using synthetic materials. Carbon
- nanotubes (32) and gold nanorods (33) have been developed but are restricted by their cytotoxicity;
- 97 silica nanorods (34) and polymeric filomicelles (31) are more biocompatible but the preparation of
- 98 well-ordered structures proves to be difficult. TMV as a nanocarrier successfully addresses these
- shortcomings because its biological nature renders high monodispersity, biocompatibility, and
- manufacturing scalability. Furthermore, TMV is unique because its length can be precisely tailored
- through its RNA cargo, and complex shapes can be directed by RNA-controlled assembly (35,36).
- 102 TMV has been harnessed for chemotherapy, photothermal immunotherapy, delivery of
- thrombolytics, as well as bioimaging and theranostic applications (37–41). The inner and outer
- surfaces of TMV are amenable to genetic manipulation or chemical conjugation via available
- tyrosine and glutamic acid residues (42). The well-established T158K mutant (TMVLys) yields
- addressable, solvent-exposed lysine residues for further functionalization (43,44). Although TMV
- proves an appealing nanocarrier for biomedical applications, the half-life of 'naked' TMV being 3.5
- proves an appearing nanocarrier for bonneau applications, the nan line of naked 1414 being 5.
- minutes in mice and pre-existing anti-TMV antibodies found in humans necessitates shielding
- strategies (45,46). To address this, we developed and characterized TMV-PEG constructs considering
- PEG chains of various length and conformation, particularly linear and multivalent PEGs with
- molecular weights of 2000 Da and 5000 Da. We thoroughly examined the conjugation efficiencies of
- each PEG onto the surface of TMV and determined to which degree intraparticle crosslinking
- occurred as a function of PEG arm valency and length. We investigate how linear vs. multivalent
- PEGylation affects TMV's biological properties such as particle stability, antibody evasion, protein
- 115 corona formation, and interactions with immune cells.

2 Materials and Methods

116

117

118

2.1 Virus propagation and purification

- Tobacco mosaic virus was propagated by mechanical inoculation of *Nicotiana benthamiana* leaves
- and purified as previously described to yield ~1 mg of virus per 1 gram of infected leaf material (42).
- For all described studies, the well-characterized T158K mutant of TMV, TMVLys, was used and for

simplicity is referred to as TMV (44).

123

124

2.2 TMV conjugation with PEG

- Linear, bivalent, and 4-arm PEGs with molecular weights of MW 2000 Da and 5000 Da (Nanocs)
- were externally grafted onto TMV particles using *N*-hydroxysuccinimide (NHS)-activated esters.
- 127 MW 2000 Da and 5000 Da PEGs were dissolved in dimethyl sulfoxide (DMSO) at 250 mg mL⁻¹ and
- 128 350 mg mL⁻¹, respectively, and added to TMV at 10, 20, 40, 60 equivalents per coat protein (CP).
- The mixtures were allowed to agitate overnight at room temperature (RT). The reactions were carried
- out at 2 mg mL⁻¹ of TMV in 0.01 M potassium phosphate (KP) buffer pH 8.0, with final DMSO
- concentration not exceeding 10% (v/v). TMV-PEG nanoparticles were purified by ultracentrifugation
- at 52,000 rpm using a TLA-55 rotor (Beckman Coulter) for 1 h on a 30% (w/v) sucrose cushion. The
- pellets were resuspended in 0.01 M KP buffer pH 7.0 and stored at 4°C. The conjugation efficiency
- of each PEG per TMV particle was quantified by densitometry analysis of protein bands in
- denaturing protein gels after staining with GelCode Blue Stain reagent (Thermo Fisher Scientific)
- using ImageJ software.

137

138

2.3 TMV conjugation with sulfo-Cy5 and O488

- To prepare fluorescent TMV formulations for imaging, remaining free lysine residues on TMV and
- 140 TMV-PEG nanoparticles were labeled with NHS-activated esters of sulfo-Cy5 (Lumiprobe) and
- Oregon Green 488-X (O488) (Invitrogen). Sulfo-Cy5 at 1.8 and 3 equivalents per CP was added to 2
- mg mL⁻¹ TMV and TMV-PEG particles, respectively, in 0.01 M KP buffer pH 8.0 containing 10%
- 143 (v/v) DMSO. For O488, 3.25 and 6.5 equivalents per CP was added to TMV and TMV-PEG,
- respectively. The reactions were carried out in the dark with agitation overnight at RT and purified
- via ultracentrifugation. Excess dye was further removed using a 100 kDa molecular weight cutoff
- 146 (MWCO) centrifugal filter unit (Millipore) until a clear flow through was achieved. Dye loading per
- particle was quantified using UV/visible spectroscopy and the specific extinction coefficient for
- sulfo-Cy5 ($\varepsilon_{647 \text{ nm}} = 271\ 000\ \text{L mol}^{-1}\ \text{cm}^{-1}$) and O488 ($\varepsilon_{496 \text{ nm}} = 70\ 000\ \text{L mol}^{-1}\ \text{cm}^{-1}$).

149

150

2.4 Ultraviolet/Visible (UV-Vis) spectroscopy

- Protein concentrations were determined using a NanoDrop 2000 spectrophotometer (Thermo
- 152 Scientific). Concentration of TMV in each sample was calculated using the Beer-Lambert law and
- 153 the extinction coefficient of TMV at 260 nm (3 mg⁻¹ mL cm⁻¹). A ratio of 260 nm to 280 nm
- absorbance of ~1.2 was used to confirm structural integrity of TMV and TMV-PEG particles.

155

156

2.5 Sodium Dodecyl Sulfate-Polyacrylamide Gel Electrophoresis (SDS-PAGE)

- 157 TMV and TMV-PEG particles (10 µg) were denatured in gel loading buffer (1 X lithium dodecyl
- sulfate sample buffer, Life Technologies with 1 X NuPAGE sample reducing agent, Invitrogen in
- 0.01 M KP buffer) and boiled at 100°C for 5 min. Protein samples and standards (SeeBlue Plus2 pre-
- stained protein standards, Invitrogen) were loaded on 4-12% or 12% NuPAGE gels (Thermo Fisher
- Scientific) and ran in 1 X MOPS buffer at 200 V and 120 mA for 35 min. Protein bands were
- visualized using GelCode Blue Stain reagent (Thermo Fisher Scientific) and imaged under a
- FluorChem E system (ProteinSimple). Cy5 and O488-labeled TMV and TMV-PEG particles were

- analyzed and imaged under the 620/40 nm Red light and 460/40 nm Blue light setting on the
- 165 FluorChem E system, respectively.

167

2.6 Dynamic Light Scattering (DLS) and ζ-Potential

- 168 The hydrodynamic diameter and ζ-potential of TMV and TMV-PEG particles were measured using a
- 169 Zetasizer Nano ZSP Zen 5600 instrument (Malvern Panalytical) and a scattering angle of 90°. The
- samples were diluted to 1 mg mL⁻¹ in 0.01 M KP and deionized water for DLS and ζ-potential,
- respectively, and ran at RT.

172

173

2.7 Transmission Electron Microscopy (TEM)

- 174 TMV and TMV-PEG particles (15 μ L at 0.5-1 mg mL⁻¹) were negatively stained with 2% (v/v)
- uranyl acetate (Electron Microscopy Sciences) for 1.5 min on a Formvar/carbon coated copper grid
- 176 (Electron Microscopy Sciences). Samples were visualized using a JEOL 1400 Plus transmission
- electron microscope at 120 kV.

178

179

2.8 Immuno dot-blots

- 180 3 μL of rabbit polyclonal α-TMV antibody (Agdia) and rabbit polyclonal α-CPMV antibody (Pacific
- Immunology) at 50 μg mL⁻¹ and rat monoclonal α-PEG antibody (BioVision) at 100 μg mL⁻¹ were
- spotted on a nitrocellulose membrane. The blots were briefly dried and blocked in 5% (w/v) bovine
- serum albumin (BSA) (Sigma-Aldrich) in PBS overnight at 4°C. The blots were then washed three
- times for 5 min each in PBS and incubated with 5 μg mL⁻¹ Cy5-labeled particles in 5% (w/v) BSA in
- PBS for 2 h at RT. After the blots were subsequently washed in PBS-T three times for 15 min each
- and a final wash in PBS for 5 min, blots were dried and imaged for fluorescence using a FluorChem
- 187 E system (ProteinSimple).

188

189

2.9 Protein corona analysis on TMV vs. TMV-PEG

- To form hard protein coronas, TMV and TMV-PEG were incubated in 2 mL 100% human plasma
- 191 (Sigma-Aldrich) in dH₂O at 0.3 mg mL⁻¹ VNPs for 1 h at RT with agitation. The samples were
- diluted in 18 ml PBS and purified by ultracentrifugation at 42,000 rpm using a 50.2 Ti rotor
- 193 (Beckman Coulter) for 2.5 h on a 40% (w/v) sucrose cushion. The pellets were washed twice with 20
- mL PBS to remove loosely bound proteins. The samples were denatured in 100-150 µL gel loading
- buffer, and proteins were separated and visualized by SDS-PAGE as previously mentioned.

196

197

2.10 Flow cytometry

- 198 RAW 264.7 murine macrophages (ATCC) in DMEM (Corning) containing 10% (v/v) FBS and 1%
- 199 (v/v) penicillin/streptomycin at 37°C and 5% CO₂ were grown to confluency and seeded into T-25
- 200 flasks at 1.5 x 10⁶ cells per flask and allowed to adhere overnight. For the TMV–cell interaction
- assay, 500,000 virions cell⁻¹ were added to each flask and incubated for 24 h at 37°C and 5% CO₂.
- To remove free VNPs, the cells were washed with PBS. The cells were gently scraped and spun
- 203 down at 500 x g for 5 min, resuspended in PBS, and transferred to a 96-well v-bottom plate. The cells
- were spun down at 300 x g for 5 min between each following step. Cells were washed again in PBS

- 205 and then fixed in 100 μL 4% (v/v) paraformaldehyde (PFA) (Electron Microscopy Sciences) in PBS
- for 10 min at RT. Following fixation, the cells were washed twice in PBS and resuspended in 200 µL 206
- 207 FACS buffer (2% (v/v) FBS, 0.09% (w/v) sodium azide (Sigma-Aldrich) in PBS). Cells were
- analyzed using a BD Accuri C6 Plus Flow Cytometer and 50,000 events were collected. Data were 208
- 209 analyzed using FlowJo v10.8.1 software. All experiments were done in triplicate.

211

2.11 Confocal microscopy

- 212 To gain insight into whether TMV or TMV-PEG are membrane-bound or internalized by
- macrophages, confocal microscopy was performed. RAW 264.7 murine macrophages were seeded at 213
- 214 1 x 10⁵ cells mL⁻¹ on 18 mm glass coverslips in a 12-well plate and allowed to attach overnight in
- 215 Dulbecco's Modified Eagle Medium (DMEM, Corning) containing 10% (v/v) fetal bovine serum
- 216 (FBS) and 1% (v/v) penicillin/streptomycin at 37°C and 5% CO₂. 500,000 virions cell⁻¹ was added to
- 217 each well and incubated for 24 h at 37°C. The cells were then fixed with 5% (v/v) PFA (Electron
- 218 Microscopy Sciences) for 10 min at RT. 5% (v/v) goat serum albumin (GSA) was used to dilute all
- 219 staining agents. Following fixation, cell membranes were stained with 1:1000 Alexa Fluor 555-
- 220 conjugated wheat germ agglutinin (WGA, Invitrogen) for 20 min at RT. The cells were then
- 221 permeabilized with 0.2% (v/v) Triton X-100 for 2 min followed by blocking in 10% (v/v) goat serum
- 222 in PBS for 1 h at RT. TMV particles were stained using 1:500 rabbit polyclonal α-TMV antibody
- (Agdia) for 2 h at RT and 1:2000 Alexa Fluor 647-conjugated goat anti-rabbit secondary antibody for 223
- 224 1 h at RT. The cells were washed thrice in PBS between each step. Coverslips were mounted onto
- 225 slides using Fluoroshield with DAPI (Sigma-Aldrich) and imaged using a Nikon A1R confocal
- 226 microscope with a 100X oil objective. Images were analyzed using Nikon NIS-Elements software.

227

228

229

Results and Discussion 3

3.1 Synthesis and characterization of PEGylated TMV constructs

- 230 TMV is a proteinaceous high-aspect ratio 300 nm x 18 nm nanorod composed of 2130 identical coat
- 231 proteins with a molecular weight of 17.5 kDa (42). For this study, TMVLys was used; TMVLys is a
- 232 well-characterized T158K TMV mutant, shown in Figure 1A, that has solvent-exposed lysine side
- 233 chains for chemical addressability. Linear and multivalent PEGs and fluorescent dyes (Sulfo-Cy5 and
- 234 Oregon Green 488) were conjugated to TMVLys using N-hydroxysuccinimide (NHS) activated
- 235 esters (Figure 1B).
- 236 To explore PEG length and conformation and their role in shielding from immune recognition, linear,
- bivalent, and 4-arm PEGs of MW 2000 or 5000 Da were conjugated to TMV (Figure 1C). While 237
- 238 linear PEG coatings on TMV have been reported, bivalent and 4-arm PEG coatings have not yet been
- 239 explored (47). The multi-arm PEGs have multiple NHS handles that can interact with TMV coat
- 240 proteins – intraparticle crosslinking can lead to a denser packing closer to the surface of TMV. We
- 241 hypothesize that such denser coatings would provide benefits in shielding as was shown previously
- for potato virus X (PVX) (48). Furthermore, multivalent PEG coatings have been demonstrated to 242
- 243 avoid the accelerated blood clearance (ABC) phenomenon and produce less anti-PEG IgM levels 244
- than their linear counterparts (49,50). By the same token, we aimed to parse out whether the
- multivalent PEG coatings on the surface of TMV could achieve more efficacious particle shielding. 245
- To maximize PEG grafting density on TMV, conjugation using molar excesses of 10:1, 20:1, 40:1, 246
- and 60:1 PEG to CP ratios were tested. PEGylation to TMV was quantified by SDS-PAGE band 247

densitometry analysis from three independent experiments (Figure 2A), and a representative SDS-PAGE gel of the TMV-PEG formulations is shown in Figure 2B. All gels used to analyze PEG conjugation in Figure 2 are pictured in Figure S1. TMV-PEG formulations were abbreviated as following: 2L = TMV-PEG2K-Linear, 2B = TMV-PEG2K-Bivalent, 2R = TMV-PEG2K-4arm, 5L = TMV-PEG5K-Linear, 5B = TMV-PEG5K-Bivalent, 5R = TMV-PEG5K-4arm. SDS-PAGE shows the characteristic CP band of TMV at 17.5 kDa (Figure 2B); PEGylation results in additional bands of higher molecular weight, which are single CP monomers with PEG (~19.5 kDa and ~22.5 kDa bands), interlinked CP dimers (~37 kDa and ~40 kDa bands), interlinked CP trimers (~54.5 kDa and ~57.5 kDa), or interlinked CP tetramers (~72 kDa and ~75 kDa), confirming the covalent attachment of the linear and multivalent PEG 2000 and 5000, respectively. It is of note that a ~75 kDa band indicating interlinked CP tetramers with 4-arm PEG 5000 is not present in Figure 2B but is shown faintly in gels used to calculate PEG grafting (Figure S1); this discrepancy is likely explained by incomplete staining of the gel in Figure 2B. Linear PEGs primarily result in CPs and CP-PEGs; however, a small ratio of dimers is also detectable (3% and 1% for PEG 2000 and 5000, respectively) most likely due to entanglement of two neighboring coat proteins – this is a consistent phenomenon and has been observed before (51,52). For the bivalent and 4-arm PEGs, a higher degree of dimers and multimeric CP bands is observed as expected as multivalent PEG handles can covalently link multiple TMV coat proteins together leading to more CP entanglement.

248

249250

251252

253254

255

256257

258

259

260

261

262

263264

265266267

268269

270

271272

273

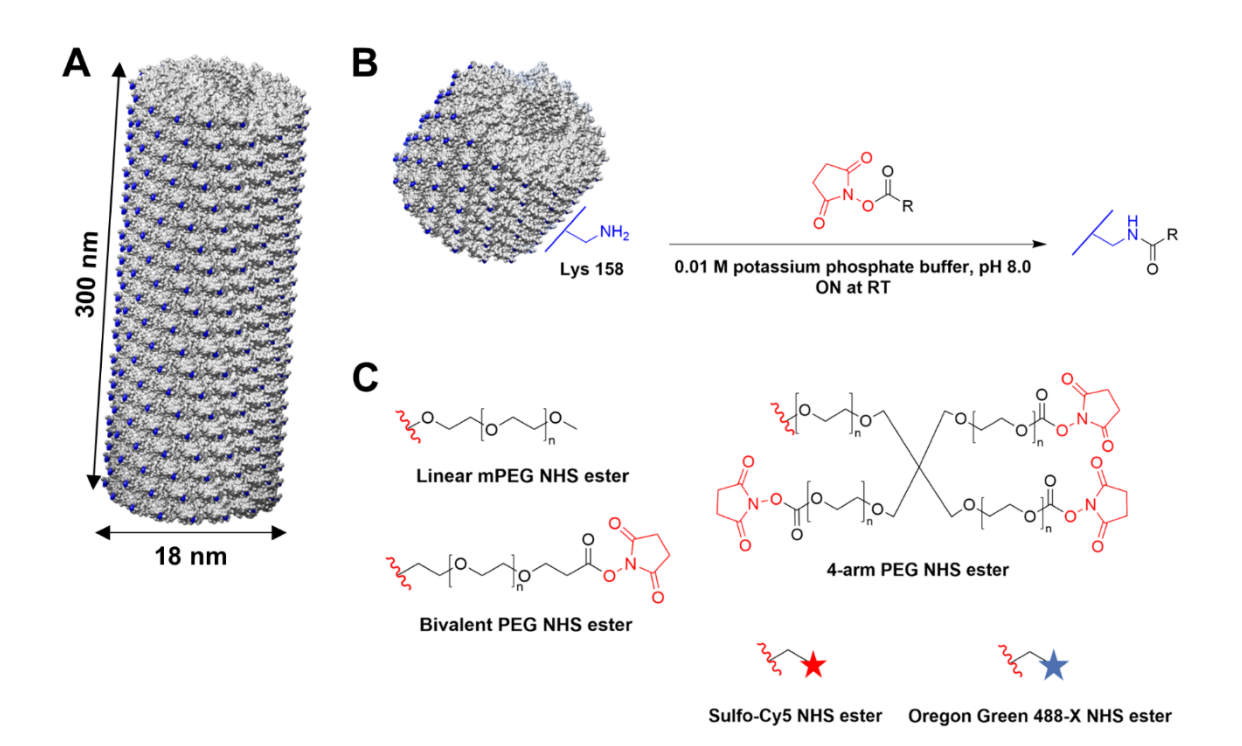


Figure 1. Chemical modification of TMV. (A) Atomic model of TMVLys, a T158K mutant of TMV. One virion composes of 2130 identical coat proteins with solvent-exposed lysine residues shown in blue. Atomic models were created on UCSF Chimera (53). (B) Schematic of external conjugation of PEGs and fluorescent dyes to lysine residues using NHS-activated esters. R denotes the target molecule. ON = overnight. (C) Conjugation reagents (Linear, Bivalent, and 4-arm PEG, Sulfo-Cy5, and Oregon Green 488-X) where the red wavy line denotes the leaving group.

For linear PEG 2000 and 5000, the conjugation efficiency plateaus near 38% and 32%, respectively, at a molar excess of 40:1 CP (**Figure 2A**). With 2130 TMV coat proteins, this equates to ~809 and ~682 linear PEG 2000 and PEG 5000 conjugated per particle, respectively. For the bivalent PEGs, optimal PEG grafting was determined at a molar excess of 20:1 CP as PEGylation drops at higher molar excesses. While 4-arm PEG 2000 grafting is maximum (~21%) at 60:1 CP, 4-arm PEG 5000 conjugation efficiency plateaus near 34% at 40:1 CP. Optimal molar excesses of PEG were used for the remainder of this study and determined by a consideration of conjugation efficiency, standard deviation, and minimization of amount of PEG used. Specifically, 40:1 CP for 2L and 5L, 20:1 CP for 2B and 5B, 60:1 CP for 2R, and 40:1 CP for 5R. However, it should be noted that overall 20:1 excess of PEG to CP was sufficient to reach maximum labeling; only the 5L formulation required a higher excess of PEG. This may be explained by the longer and linear PEG chain being more entangled therefore making the NHS reactive group less accessible.

Quantitative analysis of higher order PEGylation is shown in Figure 2C. Each TMV-PEG formulation has at least ~20% modification, with 2L having the highest percent modification at ~40% (809 labels). PEG grafting is likely limited by the effects of steric hindrance, and our results are in good agreement with Lee et al.'s estimation of 25-50% PEG conjugation efficiency onto PVX, another high aspect ratio plant virus, in which it was estimated one grafted PEG for every three CP residues (48). Interestingly, the multivalent PEG 5000 formulations had ~14-17% higher labeling than its PEG 2000 counterparts. 5B averaged ~767 PEG per TMV vs. ~405 PEG per TMV for 2B, and 5R averaged ~713 PEG per TMV vs. ~416 PEG per TMV for 2R, particularly forming a higher number of PEGylated dimers (~262 more for 5B and ~232 more for 5R than 2B and 2R, respectively). This could possibly be explained by PEG 5000 having longer 'arms' to bypass the steric hindrance of the initial attachment site and link a distal coat protein. Considering stretched out PEG, 5B displays an arm length of 39 nm vs. 16 nm for 2B, while 5R displays an arm length of 10 nm per arm vs. 4 nm per arm for 2R. The Flory dimension (R_F) of 5B is estimated to be 5.9 nm vs. 3.4 nm for 2B, and the R_F of 5R is 3.4 nm vs. 2 nm for 2R. The 300 x 18 nm TMV rod has a surface area of $A_{TMV} = 17,465 \text{ nm}^2$ with each of the 2130 CPs providing a surface area of $A_{CP} = 8.2 \text{ nm}^2$. Assuming the TMV CP is a square, the distance between two lysine residues is estimated to be 2.9 nm. The multivalent PEG 5000 formulations provide longer arm lengths and larger R_F that could better facilitate interactions with neighboring lysine residues from the initial PEG attachment site contributing to higher numbers of interlinked CP dimers.

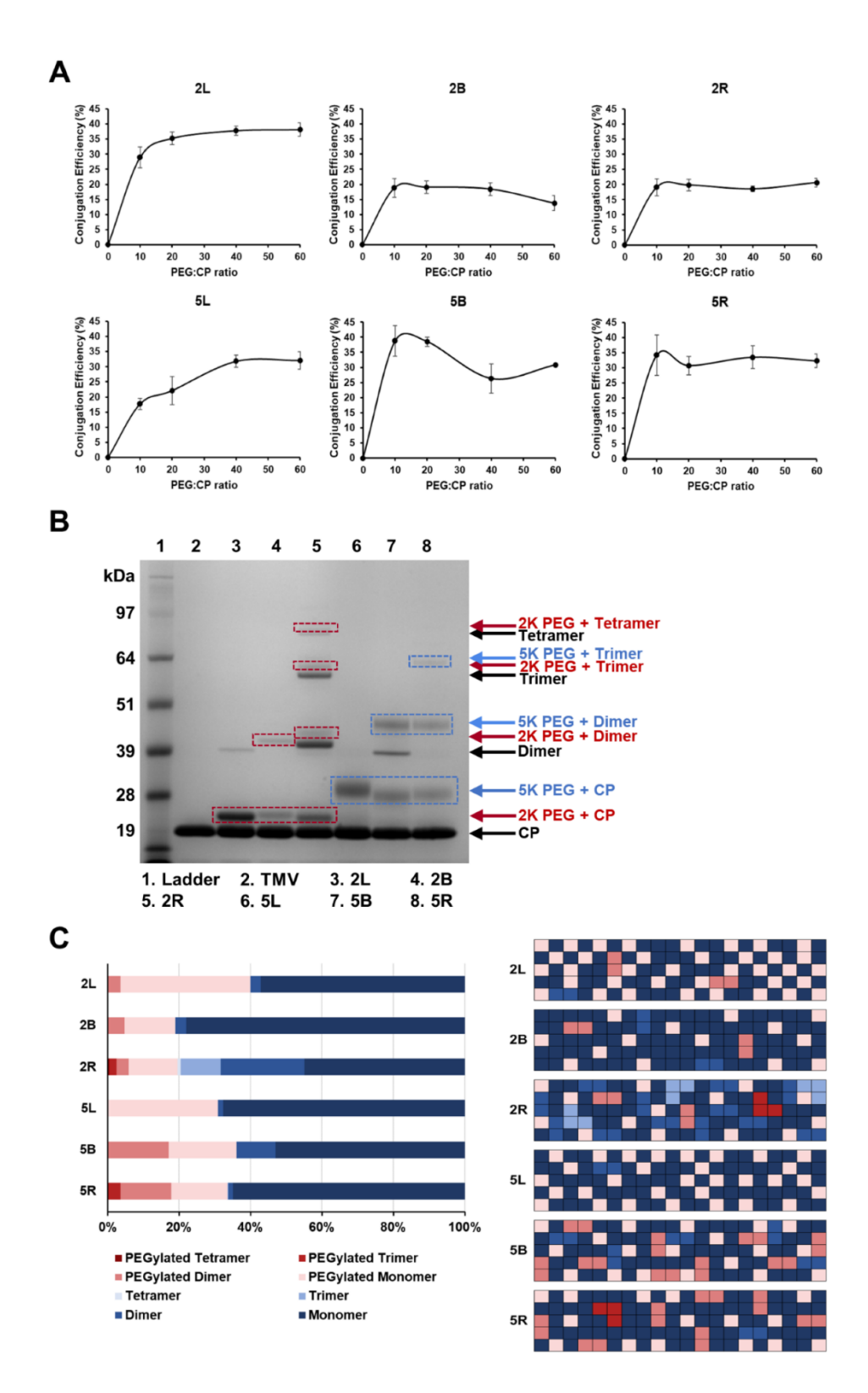


Figure 2. PEGylation of TMV nanoparticles. (A) Quantification of PEG grafting to TMV CPs as a function of molar excess used. Values were averaged from three independent experiments; error bars represent the standard deviation. (B) Representative SDS-PAGE gel of the PEGylated TMV particles. Molecular weight bands above the CP, dimer, trimer, and tetramer bands indicates PEG 2K (red boxes) or PEG 5K (blue boxes) conjugation. (C) Percentage of TMV that is grafted vs. ungrafted

- for each PEG (n = 3) quantified by densitometry analysis (left). Graphical representation of
- percentage of TMV that is grafted vs. ungrafted (right). TMV-PEG formulations were abbreviated as
- following: 2L = TMV-PEG2K-Linear, 2B = TMV-PEG2K-Bivalent, 2R = TMV-PEG2K-4arm, 5L =
- TMV-PEG5K-Linear, 5B = TMV-PEG5K-Bivalent, 5R = TMV-PEG5K-4arm.

- Purified TMV-PEG nanoparticles were characterized by ultraviolet-visible spectroscopy (UV-Vis),
- dynamic light scattering (DLS), zeta-potential measurements, and transmission electron microscopy
- 326 (TEM) to confirm structural integrity. Using the UV-Vis spectra of the TMV-PEG formulations
- 327 (Figure 3A), the 260 nm and 280 nm absorbances, corresponding to RNA and protein signals of the
- particles, respectively, were measured. A 260:280 nm ratio of 1.2 indicates pure, intact solution of
- 329 TMV (42). Indeed, all formulations present a 260:280 nm ratio near 1.2. This is consistent also with
- the SDS-PAGE where no protein contaminants were detectable.
- The particles were then characterized by DLS (**Figure 3B-C**); it is important to note that DLS is not
- accurate for sizing of high aspect ratio materials, but useful to analyze relative trends. The z-average
- of the particles ranged from 181 nm for uncoated TMV to up to 266 nm for the 5R formulation. DLS
- measurements confirm a significant increase in size for the 2R, 5L, 5B, and 5R formulations. The
- most significant size increase was observed for 2R, 5B, and 5R (p < 0.0001). It is plausible that
- longer and multivalent PEG grafting alters the surface structure of TMV such that its translational
- diffusion speed is reduced resulting in a larger hydrodynamic diameter (54); increases in
- 338 hydrodynamic diameter upon PEGylation (MW 5000) on nanoparticles have also been reported (55).
- 339 All TMV-PEG formulations were found to be monodispersed, dispersity values ranging from 0.232-
- 340 0.272, with negligible aggregation as shown in the DLS spectra (**Figure 4B**). Although it is plausible
- that the multivalent PEGs could crosslink multiple TMV particles contributing to aggregation, TEM
- imaging indicates that interparticle crosslinking was not apparent for any of the formulations (**Figure**)
- 343 **S2**, **Figure S3**).
- Zeta-potential measurements indicate that TMV (for this study, TMVLys was used) exhibits a
- surface charge of -37 mV (**Figure 3C**); it seems as the true zeta-potential of TMVLys remains
- ambiguous as other studies have reported a surface charge of ~-60 mV and -14.5 mV, and there may
- have been differences in experimental procedure such as particle concentration and solution (56,57).
- 348 Thus, zeta-potential measurements here will be used to compare relative trends only. For all
- formulations, PEGylation led to a less negative zeta-potential demonstrating a reduction in overall
- negative surface charge consistent with other reports (58,59); this can be explained by PEG coatings
- shifting the position of the slipping/shear plane outward from the particle surface resulting in a
- weaker electrostatic potential (60). Increases in PEG grafting density and length have been shown to
- reduce zeta-potential (60); 2L, the formulation with the greatest amount of PEGylation, displays a
- surface charge of -19 mV, resulting in a ~50% reduction in zeta-potential compared to native
- 355 TMVLys. No clear trend is observed between PEG chain length or conformation and zeta-potential in
- **Figure 3C**.
- In addition to the structural characterization, we confirmed thermal and chemical stability of the
- 358 TMV formulations; the PEG coatings did not impact stability of TMV and all formulations remained
- 359 structurally sound when stored in buffer mixtures for up to one week at 4°C to 37°C and in 50% (v/v)
- 360 DMSO for up to 24 hours (**Figure S2**).

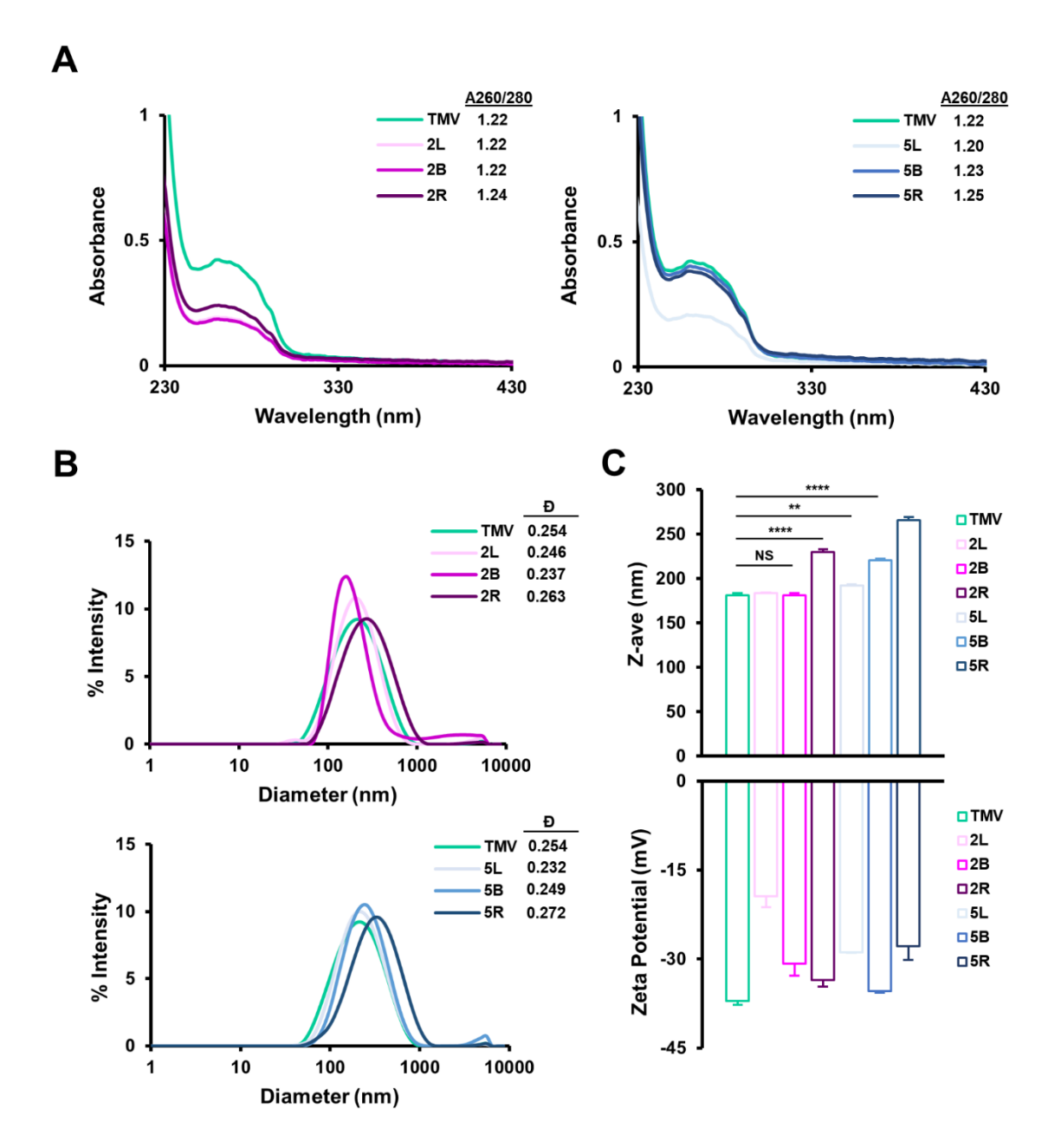


Figure 3. Characterization of TMV-PEG particles. (A) UV-Vis spectra and 260/280 nm absorbance ratios of TMV-PEG2K (left) and TMV-PEG5K (right) particles. (B) DLS spectra of TMV-PEG2K (top) and TMV-PEG5K (bottom) particles. (C) Z-average (top) and zeta-potential (bottom) measurements for each virus formulation. Statistical analyses were performed using one-way ANOVA with Tukey's multiple comparison test. ** p < 0.01, **** p < 0.0001, NS = not significant.

3.2 Biological properties of PEGylated TMV

A primary challenge to viral-based NP delivery methods is neutralization and opsonization by antibodies in which antibodies bind and biologically inactivate viruses or tag them for clearance by

phagocytic cells, respectively. PEGylation of (viral) NPs can prevent immune recognition by antibodies (48,61). To investigate whether and to what degree PEG coatings on TMV exhibit immune shielding, immune dot-blots were performed. Immune dot-blots were prepared by spotting α -TMV, α -CPMV, and α -PEG antibodies in triplicate on a nitrocellulose membrane. α -Cowpea mosaic virus (CPMV) antibodies were used as a negative control as there are no structural similarities between CPMV and TMV (51). Upon blocking the membranes with 5% (w/v) BSA, fluorescent Cy5-labeled TMV and TMV-PEG particles were incubated; the characterization of dual labeled Cy5-TMV-PEG particles are included in **Figure S3**. The membranes were then washed, dried, and analyzed. This method is preferred over blotting the nanoparticles directly onto the membrane following by addition of antibodies; the indirect capture via immobilized antibodies helps to avoid protein spreading on the nitrocellulose membrane which may induce conformational changes in PEG coatings; a schematic of the protocol is shown in Figure 4A. Antibody recognition was determined based on fluorescence readout using a FluorChem E system and quantified by densitometry analysis of the blots using ImageJ.

Based on densitometry analysis of the dot-blots (Figure 4C), PEG 5000 in any conformation, but not the PEG 2000, formulations provided shielding benefits by reducing the binding of α-TMV antibodies to TMV. Data suggest that molecular weight generally plays a larger role in antibody shielding than conformation, but it is important to note that the statistical significance of antibody shielding decreases as multivalency in PEG 5000 increased. Grafting density also likely plays a role as the multivalent PEG 5000 formulations have ~14-17% more coverage than their PEG 2000 counterparts; however, 2L has the greatest grafting density (~40%) yet does not impart antibody shielding (**Figure 2C**). Thus, the effects of PEG grafting density on α -TMV shielding remain elusive and merit further research. Further studies comparing PEG coatings at similar grafting densities or exploring PEGs with a longer backbone are likely necessary to better understand and overcome antibody recognition of the nanoparticle.

Interestingly, α -PEG recognition of the PEG 2000 formulations was strikingly lower than the PEG 5000 formulations (**Figure 4D**). This is likely attributed by the α -PEG antibody used detecting the linear backbone of PEG, in which case the PEG 5000 formulations have a ~2.5 times longer backbone than PEG 2000 allowing for better access for binding. This has implications in rising pre-existing α -PEG antibodies due to the extensive use of PEG in cosmetic products (62). Therefore, the data present an interesting balance between immune shielding of the nanoparticle and PEG itself that needs to be met if PEGylation approaches are utilized. The bivalent and 4-arm PEGs reduce α -PEG antibody recognition compared to the linear counterparts (**Figure 4D**) implying that branched PEG structures yield a different conformation in which α -PEG antibodies cannot recognize the PEG backbone as readily. This suggests that branched PEG formulations on NPs may be recommended in reducing antigenicity. This data build on other studies in which a PEG formulation of lower MW while also providing sufficient immune shielding would be ideal in clinically relevant applications (51). The data altogether though suggest that the 5B formulation provides the best balance between α -TMV and α -PEG immune shielding.

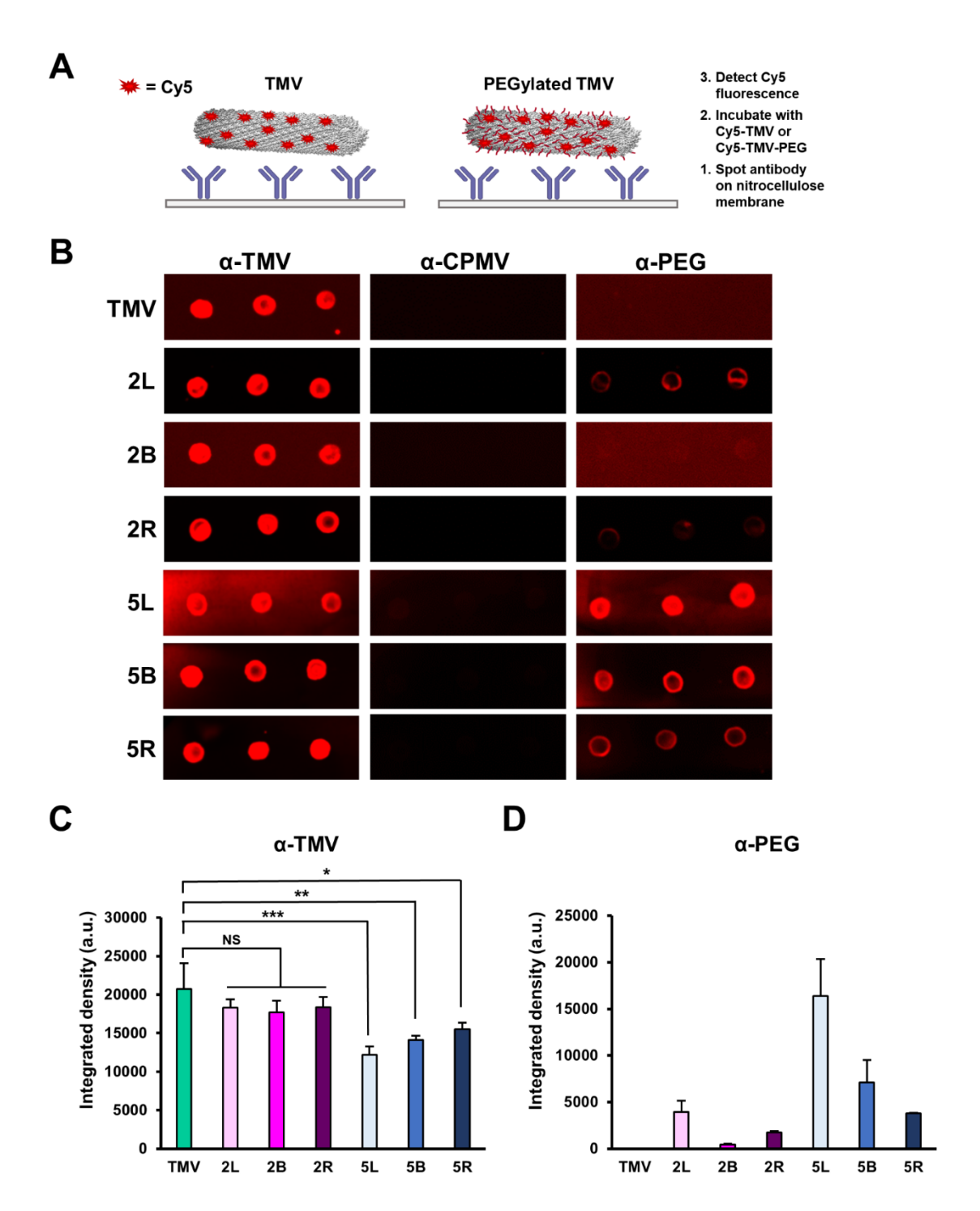


Figure 4. Immune recognition of TMV-PEG constructs. (A) Schematic of the immune dot-blot protocol to detect antibody recognition of TMV and TMV-PEG constructs. (B) Dot blots of α-TMV, α-CPMV, and α-PEG recognition of fluorescent TMV-PEG constructs. (C) Densitometry quantification of fluorescent TMV signal corresponding to antibody recognition by α-TMV antibodies from (A). (D) Densitometry quantification of fluorescent TMV signal corresponding to antibody recognition by α-PEG antibodies from (A). Statistical analyses were performed using one-way ANOVA with Tukey's multiple comparison test. * p < 0.05, ** p < 0.01, *** p < 0.001, NS = not significant.

Next, we analyzed the protein corona. When nanoparticles enter the bloodstream, serum proteins readily recognize the NPs and adsorb to the surface, forming a protein corona. The protein corona inevitably plays a role in NP biological fate and may pose another biological barrier to delivery as the protein corona may specifically or non-specifically increase uptake of NPs in non-target cells, reduce circulation time, and weaken targeting capabilities of functionalized NPs (20). Previous work from our lab have demonstrated that the protein corona of plant virus nanoparticles presents an abundance of immune system proteins, such as complement proteins and immunoglobulins, which would likely contribute to VNP clearance (57). PEG grafting is known to reduce protein adsorption on the surface of NPs, as the hydrophilic nature of PEG facilitates a hydrated cloud that sterically hinders blood components (20). To test whether PEGylation of TMV reduces or alters the protein corona surrounding TMV, we incubated the particles in ≈100% human plasma and allowed the protein corona to form. Protein corona can be segregated into hard vs. soft corona which is determined by affinity of the adsorbed proteins on the nanoparticle surface; the soft corona is constituted by proteins that are loosely bound to the NP surface while proteins of the hard corona are tightly and often irreversibly bound (63). Upon protein corona formation, the samples were briefly washed to remove the soft corona (see Methods); only the hard protein corona was considered for analysis as the proteins directly adsorb to the NP surface for prolonged periods and largely dictate biological properties of the NP (57).

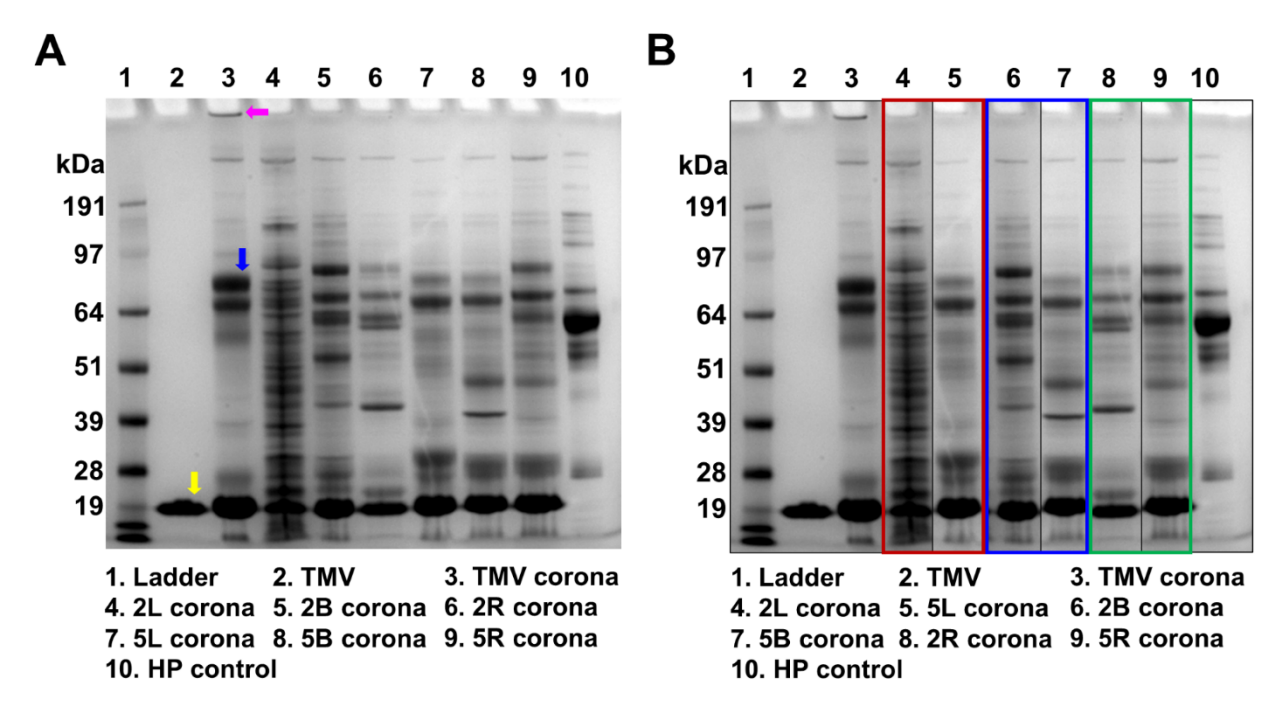


Figure 5. The protein corona of uncoated TMV and TMV-PEG constructs. (A) SDS-PAGE analysis of the protein corona formed around the VNPs after incubating the VNPs in $\approx 100\%$ human plasma for 1 hr at RT. The yellow arrow indicates the TMV coat protein. The pink arrow indicates the band of aggregation in the 'naked' TMV protein corona. The blue arrow indicates the ≈ 70 kDa protein band (complement C3/C4, plasminogen, and IgM). (B) SDS-PAGE analysis of the gel in (A) organized by PEG multivalency: linear (red box), bivalent (blue box), and 4-arm (green box). HP =

452 human plasma. 453 454 455 SDS-PAGE analysis confirms that TMV indeed acquires a protein corona (Figure 5A) with profiles as previously published (57). PEG grafting does not eliminate protein adsorption; rather, each TMV-456 457 PEG formulation presents a slightly different protein corona composition. Notably, for the 'naked' TMV – large aggregates are detected in the well of the gel. This aggregation is not apparent for the 458 459 PEGylated TMV samples. Furthermore, the ≈70 kDa band has previously been identified to compose 460 of complement protein C3/C4, plasminogen, and IgM (57); the protein corona of the 2L, 2B, 2R, and 461 5R do not contain this band which suggests that PEGylation has prevented adsorption of these serum 462 proteins. While the protein corona of 5L and 5B seem to present this ≈70 kDa band, it is at a much 463 lower intensity compared to the corona of TMV. 464 In Figure 5B, the lanes are organized by PEG valency instead of molecular weight. 2L and 5L's 465 corona composition widely differ, so it is likely the conformation of these PEGs is distinct and 466 affects the interaction with serum proteins. The protein corona of 2B and 5B do not pose striking 467 differences. Interestingly, the protein corona of 2R and 5R are the most similar, implying that the 468 structure-function of these PEGs are comparable in serum protein interactions. While insightful, this 469 protein corona study only gives a qualitative understanding of the protein corona of uncoated vs. 470 PEGylated TMV. To gain a more quantitative understanding of protein corona abundance and 471 composition for each virus formulation, mass spectrometry analysis would be required, as has been 472 previously described (64.65). 473 474 475

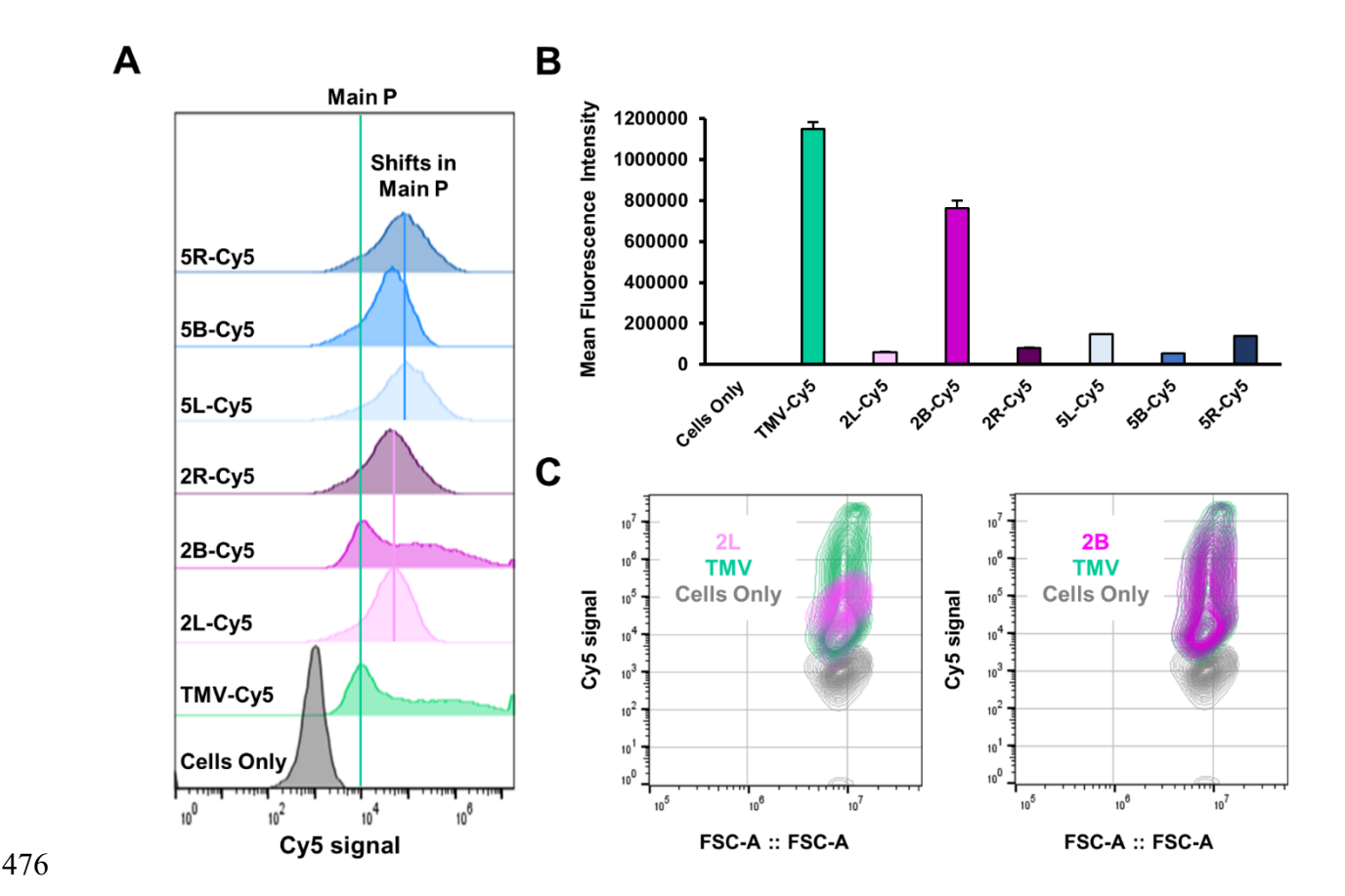


Figure 6. In vitro cellular interactions between TMV-PEG and RAW 264.7 macrophages. (A) Flow cytometry histograms of macrophage uptake of 'naked' and PEGylated TMV constructs. The particles were tracked by conjugated Cy5 fluorophores. The green line indicates the main peak of Cy5 signal from TMV, while the pink and blue lines indicate peak shifts in PEG 2000 and PEG 5000 formulations, respectively. (B) Quantitative flow cytometry analysis of the same constructs in (A). (C) Contour plots of 2L uptake (left) and 2B uptake (right).

Lastly, we assayed the effects of PEGylation on TMV-immune cell interactions. Systemically administered NPs are often prematurely cleared by the mononuclear phagocytic system (MPS) (20); here we used RAW 264.7 murine macrophages as a model system for phagocytic cells and compared uptake of 'naked' and PEGylated TMV using flow cytometry and confocal microscopy. Cy5-labeled TMV was used and flow cytometry analysis confirms that TMV is taken up by macrophages (Figure 6A). Interestingly, the histogram profile of TMV shows a main peak in Cy5 signal, but a tail off the main peak is also present signaling that there is heterogeneity in the amount of TMV that the macrophages have interacted with. We speculate that the presence of the tail could indicate differences in cellular localization or non-specific uptake of the particles. With the exception of the 2B formulation, PEGylation results in main peak shifts but also the loss of the tail (Figure 6A and Figure 6C). This implies that PEGylation modulates TMV-immune cell interactions; while the PEG coatings seem to promote the uptake of TMV in the main cell population, it also reduces the heterogeneity and overall amount of particle uptake as observed in mean fluorescent intensity values (Figure 6B). Surprisingly, the 2B construct results in no significant change in macrophage

interactions and even its histogram and contour profiles (**Figure 6A and Figure 6C**) resembles 'naked' TMV's. Besides the 2B construct, no notable trends are observed between PEG conformation and macrophage interactions. The data highlight that there are nuanced structure-functional relationships in PEG conformation needed to be elucidated.

Our lab has shown that fluorescent labels can alter biophysical properties of PEGylated VNPs; specifically, the shielding effects of PVX-PEG constructs were either exhibited or lost depending on the fluorescent dye being used (66). We noted that Cy5 conjugation in particular may enhance nanoparticle-cell interactions, which may be due to interactions of the dye with the lipid membrane. To explore whether interactions between TMV-PEG and macrophages display such a dyedependency, we labeled TMV and 5R with another dye, Oregon Green O488-X (O488), and repeated the flow cytometry experiment with RAW 264.7 cells. Characterization of O488-labeled particles are shown in **Figure S4**.



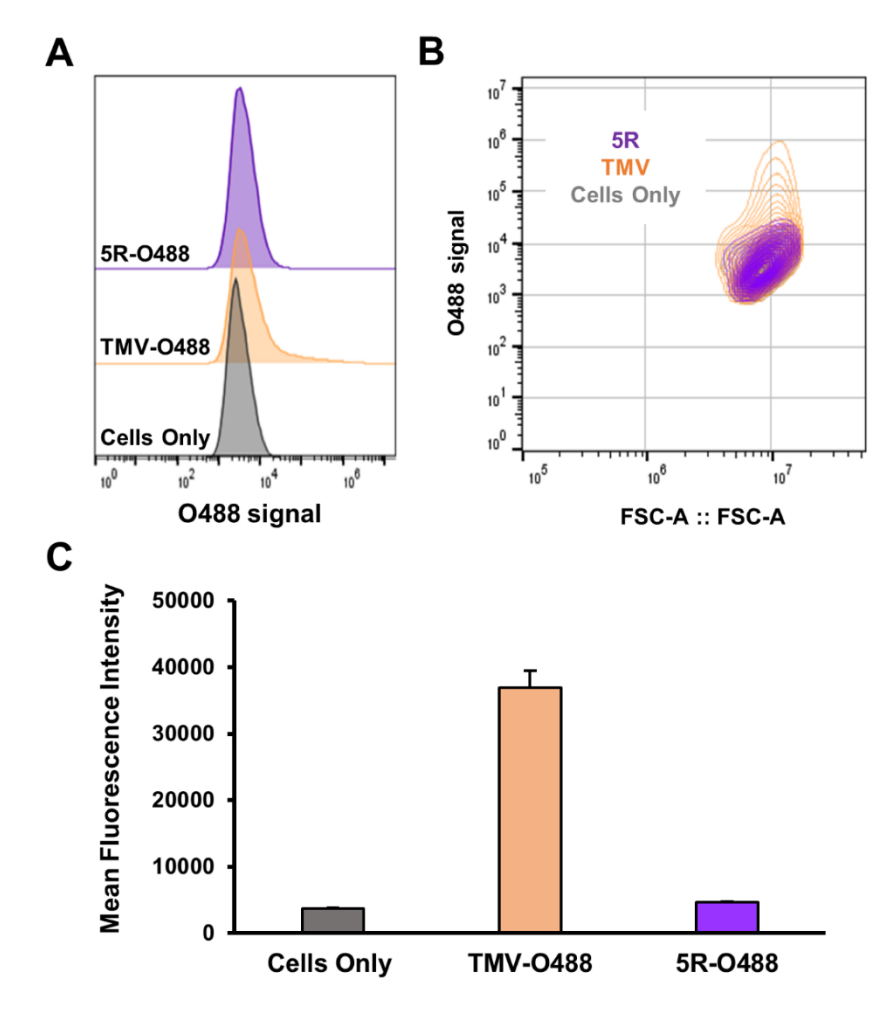


Figure 7. Evaluating O488-labeled TMV and TMV-PEG interactions with RAW 264.7 macrophages. (A) Flow cytometry histograms of RAW 264.7 macrophage uptake of O488-labeled TMV and 5R constructs. (B) Contour plots of TMV and 5R uptake. (C) Quantitative flow cytometry analysis of the same constructs in (A).

518 519 520 Some key differences were noted: overall the O488 signal was not as profound compared to Cy5 521 signals, which may be explained by differences in fluorescence intensity from the dyes. Given the 522 lower signal intensity, the main peak shift and the tail population is not as significant in TMV-O488 523 vs. TMV-Cy5 (Figure 7 vs Figure 6). 5R-O488 particles eliminate the heterogeneity in macrophage 524 uptake, leading to an overall reduction in immune cell interactions; that is the tail is lost and the main peak appears to overlap with the 'naked' TMV-O488 (Figure 7A-B). No changes, and in particular 525 no enhancement of the main population was noted for TMV-O488 – therefore this data indicates that 526 527 the Cy5 label indeed alters the cellular interaction profiles. Together this data suggests that dyelabeling can have an impact on the cell interactions of nanoparticles; globally when analyzing the 528 mean fluorescence intensity (MFI), data suggest reduced cell interactions for all but the 2B 529 formulation. However, histograms and contour plots indicate more nuanced differences between the 530 PEGylated and 'naked' TMV. 531 Therefore, to probe whether signal from the 'naked' vs. PEGylated particles in Figure 6 and Figure 532 533 7 came from internalized vs. cell membrane-bound particles, confocal microscopy was performed. 2L 534 and 2B constructs were considered for confocal microscopy because 2L, along with the remaining 535 TMV-PEG constructs, modulated TMV-macrophage interactions, but 2B did not so we aimed to 536 characterize any apparent differences between such formulations. Z-stack analysis of confocal microscopy images (Figure 8) showed that both 'naked' TMV and PEGylated formulations are 537 538 internalized by RAW 264.7 murine macrophages after 24 hours post-incubation. Furthermore, cell 539 surface binding is not specific to PEGylated particles as both native and PEGylated particles lodge 540 into the cell membrane. Time course or time-lapse studies may elucidate differences in the rate of internalization between native vs. PEGylated particles; for example, PEGylated particles may stay 541 lodged into the cell membrane longer than 'naked' TMV before being internalized. 542

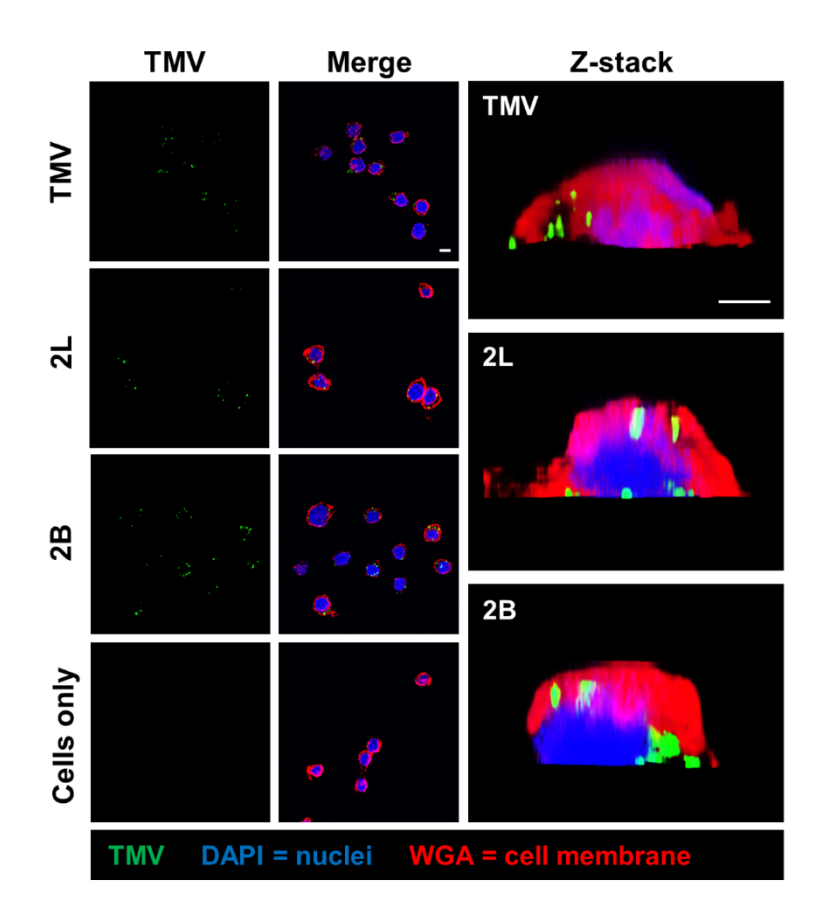


Figure 8. Cellular localization of TMV and TMV-PEG particles in RAW 264.7 macrophages. Confocal microscopy of TMV and TMV-PEG uptake by RAW 264.7 macrophages after 24 h. TMV is labeled in green, cell membrane marker WGA in red, and cell nuclei (DAPI) in blue. Z-stack cross-sections of RAW 264.7 cells are shown in the last column. Scale bars = 10 μm.

4 Conclusion

In this work, we investigated linear vs. multivalent PEG coatings to overcome immune defense mechanisms against nanoparticle delivery platforms. We demonstrated successful PEGylation of TMV, a plant virus nanoparticle widely studied as a candidate material for drug delivery, therapeutic, and bioimaging applications. Conjugation efficiencies of ~20-40% were achieved for linear, bivalent, and 4-arm PEGs of MW 2000 and 5000 Da onto TMV, and we detailed the formation of higher order PEG-oligomer structures upon multivalent PEG grafting. TMV-PEG formulations demonstrated a high degree of thermal and chemical stability with no apparent sign of broken particles or aggregation. PEG 5000, but not PEG 2000, coatings provided shielding against α -TMV antibody recognition *in vitro*, underscoring the importance of PEG chain length in NP stealthing. α -TMV antibody evasion decreased as PEG multivalency increased for the PEG 5000 formulations. Shorter, multivalent PEG coatings preferentially prevented α -PEG antibody binding which strikes an interesting balance between potential antigenicity attributed by the NP and PEG itself – this balance needs to be considered if PEGylation strategies are implemented in NP design. All PEG coatings reduced aggregation with serum proteins and yielded differences in the composition of their protein corona, particularly reducing the adsorption of complement proteins and IgM. Apart from the 2B

- construct, Cy5-labeled TMV-PEG constructs modulated interactions with macrophages, while O488-
- labeled TMV-PEG constructs presented shielding properties suggesting that biophysical
- characteristics of PEGylated TMV are sensitive to dye labeling. We report no obvious trends between
- linear vs. multivalent PEGylation in macrophage uptake and serum protein adsorption, highlighting
- 570 that each PEG has distinct structure-function relationships.

- 572 In summary, we developed linear and multivalent PEGylated plant virus nanoparticles in which PEG
- coatings contributed advantageous stealth properties. This work gives insight into NP shielding
- strategies and can be expanded to proteins and therapeutics. This study also contributes to the
- research and development of multivalent or branched PEG-grafted nanocarriers. Finally, efficient
- strategies for polymer conjugation open the door for using TMV and related virus-like particles as
- 577 high-multivalent junctions in molecularly based polymer networks. The size and aspect ratio of
- 578 TMV, in combination with the atomic precision of its structure, make it an attractive candidate for
- 579 nanoscale analogues of fiber-reinforced composites and related microscale materials. The results
- obtained here provide a foundation for future investigations of the synthesis and properties of such
- 581 materials.

582

583

Conflict of Interest

- Dr. Steinmetz is a co-founder of, has equity in, and has a financial interest with Mosaic
- 585 ImmunoEngineering Inc. Dr. Steinmetz serves as Director, Board Member, and Acting Chief
- Scientific Officer, and paid consultant to Mosaic. The other authors declare no potential COI.

587 Author Contributions

- N.F.S. and S.L.C. conceptualized the study. R.M.C., I.G.G., and N.F.S. designed the study and
- experiments. R.M.C. conducted all experiments, analyzed the data, and wrote the manuscript with
- guidance from N.F.S. All authors edited the manuscript. N.F.S. oversaw the study.

591 Funding

- This work was supported by the NSF Center for the Chemistry of Molecularly Optimized Networks
- 593 (MONET), CHE-2116298. R.M.C. was supported in part by the NSF Graduate Research Fellowship
- 594 under Grant No. DGE-2038238.

595 Acknowledgments

- The authors appreciate Andrea G. Monroy-Borrego and Anthony O. Omole for their guidance on
- 597 TMVLys propagation/purification and in vitro assays, respectively. The authors acknowledge the
- 598 University of California, San Diego Cellular and Molecular Medicine Electron Microscopy Core
- 599 (UCSD-CMM-EM Core, RRID:SCR_022039) for equipment access and technical assistance. The
- 600 UCSD-CMM-EM Core is supported in part by the National Institutes of Health Award number
- 601 S10OD023527.
- 602 Selected molecular graphics were created on Biorender.com.

603 Supplementary Material

604 605 606 607 608	Figure S1 SDS-PAGE analysis of TMV-PEG constructs	
	Figure S2 Temperature and chemical stability of TMV-PEG particles	
	Figure S3 Cy5 labeling of TMV and TMV-PEG particles	
609 610	Figure S4 O488 labeling of TMV and TMV-PEG particles	
611 612	Figure S5 Cellular localization of TMV and TMV-PEG particles in RAW 264.7 macrophages (all panels shown)	
613	Data availability statement	
614	Data will be available from the authors upon reasonable request.	
615	References	
616 617	1.	Blanco E, Shen H, Ferrari M. Principles of nanoparticle design for overcoming biological barriers to drug delivery. <i>Nat Biotechnol</i> (2015) 33:941–951. doi: 10.1038/nbt.3330
618 619 620	2.	Mitchell MJ, Billingsley MM, Haley RM, Wechsler ME, Peppas NA, Langer R. Engineering precision nanoparticles for drug delivery. <i>Nat Rev Drug Discov</i> (2021) 20:101–124. doi: 10.1038/s41573-020-0090-8
621 622 623 624	3.	Guo F, Fu Q, Zhou K, Jin C, Wu W, Ji X, Yan Q, Yang Q, Wu D, Li A, et al. Matrix metalloprotein-triggered, cell penetrating peptide-modified star-shaped nanoparticles for tumor targeting and cancer therapy. <i>J Nanobiotechnology</i> (2020) 18:48. doi: 10.1186/s12951-020-00595-5
625 626 627	4.	Rao L, Yu G, Meng Q, Bu L, Tian R, Lin L, Deng H, Yang W, Zan M, Ding J, et al. Cancer Cell Membrane-Coated Nanoparticles for Personalized Therapy in Patient-Derived Xenograft Models. <i>Adv Funct Mater</i> (2019) 29:1905671. doi: 10.1002/adfm.201905671
628 629 630	5.	Li K, Lu L, Xue C, Liu J, He Y, Zhou J, Xia Z, Dai L, Luo Z, Mao Y, et al. Polarization of tumor-associated macrophage phenotype <i>via</i> porous hollow iron nanoparticles for tumor immunotherapy <i>in vivo</i> . <i>Nanoscale</i> (2020) 12:130–144. doi: 10.1039/C9NR06505A
631 632 633	6.	Liu X, Li C, Lv J, Huang F, An Y, Shi L, Ma R. Glucose and H 2 O 2 Dual-Responsive Polymeric Micelles for the Self-Regulated Release of Insulin. <i>ACS Appl Bio Mater</i> (2020) 3:1598–1606. doi: 10.1021/acsabm.9b01185
634 635 636	7.	Clegg JR, Irani AS, Ander EW, Ludolph CM, Venkataraman AK, Zhong JX, Peppas NA. Synthetic networks with tunable responsiveness, biodegradation, and molecular recognition for precision medicine applications. <i>Sci Adv</i> (2019) 5: doi: 10.1126/sciadv.aax7946
637 638 639 640	8.	Knight FC, Gilchuk P, Kumar A, Becker KW, Sevimli S, Jacobson ME, Suryadevara N, Wang-Bishop L, Boyd KL, Crowe JE, et al. Mucosal Immunization with a pH-Responsive Nanoparticle Vaccine Induces Protective CD8 ⁺ Lung-Resident Memory T Cells. <i>ACS Nano</i> (2019) 13:10939–10960. doi: 10.1021/acsnano.9b00326

- Dölen Y, Valente M, Tagit O, Jäger E, van Dinther EAW, van Riessen NK, Hruby M, Gileadi
- U, Cerundolo V, Figdor CG. Nanovaccine administration route is critical to obtain pertinent
- iNKt cell help for robust anti-tumor T and B cell responses. *Oncoimmunology* (2020) 9: doi:
- 644 10.1080/2162402X.2020.1738813
- 645 10. Xu C, Gao F, Wu J, Niu S, Li F, Jin L, Shi Q, Du L. Biodegradable nanotheranostics with
- 646 hyperthermia-induced bubble ability for ultrasound imaging—guided chemo-photothermal
- 647 therapy. Int J Nanomedicine (2019) 14:7141–7153. doi: 10.2147/IJN.S213518
- 11. Pant K, Neuber C, Zarschler K, Wodtke J, Meister S, Haag R, Pietzsch J, Stephan H. Active
- Targeting of Dendritic Polyglycerols for Diagnostic Cancer Imaging. *Small* (2020)
- 650 16:1905013. doi: 10.1002/smll.201905013
- 651 12. Volpatti LR, Matranga MA, Cortinas AB, Delcassian D, Daniel KB, Langer R, Anderson DG.
- Glucose-Responsive Nanoparticles for Rapid and Extended Self-Regulated Insulin Delivery.
- 653 ACS Nano (2020) 14:488–497. doi: 10.1021/acsnano.9b06395
- 654 13. Gao Y, Jia L, Wang Q, Hu H, Zhao X, Chen D, Qiao M. pH/Redox Dual-Responsive Polyplex
- with Effective Endosomal Escape for Codelivery of siRNA and Doxorubicin against Drug-
- Resistant Cancer Cells. ACS Appl Mater Interfaces (2019) 11:16296–16310. doi:
- 657 10.1021/acsami.9b02016
- Lang F, Parayath NN, Ene CI, Stephan SB, Koehne AL, Coon ME, Holland EC, Stephan
- MT. Genetic programming of macrophages to perform anti-tumor functions using targeted
- mRNA nanocarriers. *Nat Commun* (2019) 10:3974. doi: 10.1038/s41467-019-11911-5
- 661 15. Wei L, Zhao Y, Hu X, Tang L. Redox-Responsive Polycondensate Neoepitope for Enhanced
- Personalized Cancer Vaccine. ACS Cent Sci (2020) 6:404–412. doi:
- 663 10.1021/acscentsci.9b01174
- 664 16. Zhang Y, Meng S, Ding J, Peng Q, Yu Y. Transition metal-coordinated graphitic carbon
- nitride dots as a sensitive and facile fluorescent probe for β-amyloid peptide detection. *Analyst*
- 666 (2019) 144:504–511. doi: 10.1039/C8AN01620H
- 667 17. Cheng Q, Wei T, Farbiak L, Johnson LT, Dilliard SA, Siegwart DJ. Selective organ targeting
- (SORT) nanoparticles for tissue-specific mRNA delivery and CRISPR—Cas gene editing. *Nat*
- Nanotechnol (2020) 15:313–320. doi: 10.1038/s41565-020-0669-6
- 670 18. Valcourt DM, Dang MN, Scully MA, Day ES. Nanoparticle-Mediated Co-Delivery of Notch-1
- Antibodies and ABT-737 as a Potent Treatment Strategy for Triple-Negative Breast Cancer.
- 672 ACS Nano (2020) 14:3378–3388. doi: 10.1021/acsnano.9b09263
- 673 19. Brown SB, Wang L, Jungels RR, Sharma B. Effects of cartilage-targeting moieties on
- nanoparticle biodistribution in healthy and osteoarthritic joints. *Acta Biomater* (2020)
- 675 101:469–483. doi: 10.1016/j.actbio.2019.10.003
- 676 20. Suk JS, Xu Q, Kim N, Hanes J, Ensign LM. PEGylation as a strategy for improving
- 677 nanoparticle-based drug and gene delivery. Adv Drug Deliv Rev (2016) 99:28–51. doi:
- 678 10.1016/j.addr.2015.09.012

- 679 21. Tenzer S, Docter D, Kuharev J, Musyanovych A, Fetz V, Hecht R, Schlenk F, Fischer D,
- Kiouptsi K, Reinhardt C, et al. Rapid formation of plasma protein corona critically affects
- nanoparticle pathophysiology. *Nat Nanotechnol* (2013) 8:772–781. doi:
- 682 10.1038/nnano.2013.181
- 683 22. Klibanov AL, Maruyama K, Torchilin VP, Huang L. Amphipathic polyethyleneglycols
- effectively prolong the circulation time of liposomes. *FEBS Lett* (1990) 268:235–237. doi:
- 685 10.1016/0014-5793(90)81016-H
- 686 23. Miteva M, Kirkbride KC, Kilchrist K v., Werfel TA, Li H, Nelson CE, Gupta MK, Giorgio
- TD, Duvall CL. Tuning PEGylation of mixed micelles to overcome intracellular and systemic
- 688 siRNA delivery barriers. *Biomaterials* (2015) 38:97–107. doi:
- 689 10.1016/j.biomaterials.2014.10.036
- 690 24. Bazile D, Prud'homme C, Bassoullet M, Marlard M, Spenlehauer G, Veillard M. Stealth Me.
- PEG-PLA Nanoparticles Avoid Uptake by the Mononuclear Phagocytes System. *J Pharm Sci*
- 692 (1995) 84:493–498. doi: 10.1002/jps.2600840420
- 693 25. Yang Q, Lai SK. Anti-PEG immunity: emergence, characteristics, and unaddressed questions.
- Wiley Interdiscip Rev Nanomed Nanobiotechnol (2015) 7:655–677. doi: 10.1002/wnan.1339
- 695 26. Swierczewska M, Lee KC, Lee S. What is the future of PEGylated therapies? Expert Opin
- 696 Emerg Drugs (2015) 20:531–536. doi: 10.1517/14728214.2015.1113254
- 697 27. Anselmo AC, Mitragotri S. Nanoparticles in the clinic: An update. *Bioeng Transl Med* (2019)
- 698 4:e10143. doi: 10.1002/btm2.10143
- 699 28. Lee KL, Hubbard LC, Hern S, Yildiz I, Gratzl M, Steinmetz NF. Shape matters: the diffusion
- rates of TMV rods and CPMV icosahedrons in a spheroid model of extracellular matrix are
- 701 distinct. *Biomater Sci* (2013) 1:581. doi: 10.1039/c3bm00191a
- 702 29. Champion JA, Mitragotri S. Role of target geometry in phagocytosis. *Proc. Natl. Acad. Sci.*
- 703 U.S.A. (2006) 103:4930–4934. doi: 10.1073/pnas.0600997103
- 704 30. Geng Y, Dalhaimer P, Cai S, Tsai R, Tewari M, Minko T, Discher DE. Shape effects of
- filaments versus spherical particles in flow and drug delivery. *Nat Nanotechnol* (2007) 2:249–
- 706 255. doi: 10.1038/nnano.2007.70
- 707 31. Lagarrigue P, Moncalvo F, Cellesi F. Non-spherical Polymeric Nanocarriers for Therapeutics:
- The Effect of Shape on Biological Systems and Drug Delivery Properties. *Pharmaceutics*
- 709 (2022) 15:32. doi: 10.3390/pharmaceutics15010032
- 710 32. Zare-Zardini H, Hatamizadeh N, Haddadzadegan N, Soltaninejad H, Karimi-Zarchi M.
- Advantages and disadvantages of using Carbon Nanostructures in Reproductive Medicine: two
- 712 sides of the same coin. *JBRA Assist Reprod* (2022) 26:142–144. doi: 10.5935/1518-
- 713 0557.20210070
- 714 33. Khan NU, Lin J, Younas MR, Liu X, Shen L. Synthesis of gold nanorods and their
- 715 performance in the field of cancer cell imaging and photothermal therapy. *Cancer*
- 716 Nanotechnol (2021) 12:20. doi: 10.1186/s12645-021-00092-w

- Jafari S, Derakhshankhah H, Alaei L, Fattahi A, Varnamkhasti BS, Saboury AA. Mesoporous
 silica nanoparticles for therapeutic/diagnostic applications. *Biomedicine & Pharmacotherapy*
- 719 (2019) 109:1100–1111. doi: 10.1016/j.biopha.2018.10.167
- 720 35. Eber FJ, Eiben S, Jeske H, Wege C. RNA-controlled assembly of tobacco mosaic virus-
- derived complex structures: from nanoboomerangs to tetrapods. *Nanoscale* (2015) 7:344–355.
- 722 doi: 10.1039/C4NR05434B
- 723 36. Wege C, Koch C. From stars to stripes: RNA-directed shaping of plant viral protein
- templates—structural synthetic virology for smart biohybrid nanostructures. WIREs
- Nanomedicine and Nanobiotechnology (2020) 12: doi: 10.1002/wnan.1591
- 726 37. Zhao Z, Simms A, Steinmetz NF. Cisplatin-Loaded Tobacco Mosaic Virus for Ovarian Cancer
- 727 Treatment. *Biomacromolecules* (2022) 23:4379–4387. doi: 10.1021/acs.biomac.2c00831
- 728 38. Shin MD, Ortega-Rivera OA, Steinmetz NF. Multivalent Display of ApoAI Peptides on the
- 729 Surface of Tobacco Mosaic Virus Nanotubes Improves Cholesterol Efflux. *Bioconjug Chem*
- 730 (2022) 33:1922–1933. doi: 10.1021/acs.bioconjchem.2c00371
- 731 39. Nkanga CI, Ortega-Rivera OA, Steinmetz NF. Photothermal immunotherapy of melanoma
- using TLR-7 agonist laden tobacco mosaic virus with polydopamine coat. *Nanomedicine*
- 733 (2022) 44:102573. doi: 10.1016/j.nano.2022.102573
- 734 40. Wu Z, Zhou J, Nkanga CI, Jin Z, He T, Borum RM, Yim W, Zhou J, Cheng Y, Xu M, et al.
- One-Step Supramolecular Multifunctional Coating on Plant Virus Nanoparticles for
- Bioimaging and Therapeutic Applications. ACS Appl Mater Interfaces (2022) 14:13692–
- 737 13702. doi: 10.1021/acsami.1c22690
- 738 41. Nkanga CI, Chung YH, Shukla S, Zhou J, Jokerst J v., Steinmetz NF. The *in vivo* fate of
- tobacco mosaic virus nanoparticle theranostic agents modified by the addition of a
- 740 polydopamine coat. *Biomater Sci* (2021) 9:7134–7150. doi: 10.1039/D1BM01113H
- 741 42. Bruckman MA, Steinmetz NF. Chemical modification of the inner and outer surfaces of
- 742 Tobacco Mosaic Virus (TMV). Methods Mol Biol (2014) 1108:173–85. doi: 10.1007/978-1-
- 743 62703-751-8 13
- 744 43. Shukla S, Eber FJ, Nagarajan AS, DiFranco NA, Schmidt N, Wen AM, Eiben S, Twyman
- RM, Wege C, Steinmetz NF. The Impact of Aspect Ratio on the Biodistribution and Tumor
- Homing of Rigid Soft-Matter Nanorods. *Adv Healthc Mater* (2015) 4:874–882. doi:
- 747 10.1002/adhm.201400641
- 748 44. Geiger FC, Eber FJ, Eiben S, Mueller A, Jeske H, Spatz JP, Wege C. TMV nanorods with
- programmed longitudinal domains of differently addressable coat proteins. *Nanoscale* (2013)
- 750 5:3808. doi: 10.1039/c3nr33724c
- 751 45. Bruckman MA, Randolph LN, VanMeter A, Hern S, Shoffstall AJ, Taurog RE, Steinmetz NF.
- Biodistribution, pharmacokinetics, and blood compatibility of native and PEGylated tobacco
- mosaic virus nano-rods and -spheres in mice. *Virology* (2014) 449:163–173. doi:
- 754 10.1016/j.virol.2013.10.035

- 755 46. Liu R, Vaishnav RA, Roberts AM, Friedland RP. Humans Have Antibodies against a Plant
- 756 Virus: Evidence from Tobacco Mosaic Virus. *PLoS One* (2013) 8:e60621. doi:
- 757 10.1371/journal.pone.0060621
- 758 47. Pitek A S., Jameson S A., Veliz F A., Shukla S, Steinmetz N F. Serum albumin 'camouflage'
- of plant virus based nanoparticles prevents their antibody recognition and enhances
- pharmacokinetics. *Biomaterials* (2016) 89:89–97. doi: 10.1016/j.biomaterials.2016.02.032
- 48. Lee KL, Shukla S, Wu M, Ayat NR, el Sanadi CE, Wen AM, Edelbrock JF, Pokorski JK,
- Commandeur U, Dubyak GR, et al. Stealth filaments: Polymer chain length and conformation
- affect the in vivo fate of PEGylated potato virus X. *Acta Biomater* (2015) 19:166–179. doi:
- 764 10.1016/j.actbio.2015.03.001
- Here Tan Hand Mark Liu M, Zhao D, Yan N, Li J, Zhang H, Liu M, Tang X, Liu X, Deng Y, Song Y, et al. Evasion
- of the accelerated blood clearance phenomenon by branched PEG lipid derivative coating of
- 767 nanoemulsions. *Int J Pharm* (2022) 612:121365. doi: 10.1016/j.ijpharm.2021.121365
- 768 50. Liu M, Li J, Zhao D, Yan N, Zhang H, Liu M, Tang X, Hu Y, Ding J, Zhang N, et al.
- Branched PEG-modification: A new strategy for nanocarriers to evade of the accelerated blood
- clearance phenomenon and enhance anti-tumor efficacy. *Biomaterials* (2022) 283:121415. doi:
- 771 10.1016/j.biomaterials.2022.121415
- 772 51. Gulati NM, Pitek AS, Czapar AE, Stewart PL, Steinmetz NF. The *in vivo* fates of plant viral
- nanoparticles camouflaged using self-proteins: overcoming immune recognition. *J Mater*
- 774 *Chem B* (2018) 6:2204–2216. doi: 10.1039/C7TB03106H
- 775 52. Pitek AS, Park J, Wang Y, Gao H, Hu H, Simon DI, Steinmetz NF. Delivery of thrombolytic
- therapy using rod-shaped plant viral nanoparticles decreases the risk of hemorrhage.
- 777 Nanoscale (2018) 10:16547–16555. doi: 10.1039/C8NR02861C
- 778 53. Pettersen EF, Goddard TD, Huang CC, Couch GS, Greenblatt DM, Meng EC, Ferrin TE.
- UCSF Chimera--a visualization system for exploratory research and analysis, *J Comput Chem*
- 780 (2004) 25:1605–12. doi: 10.1002/jcc.20084
- 781 54. Malvern Instruments. Dynamic Light Scattering: An Introduction in 30 Minutes. *DLS*
- 782 *Technical Note, MRK656* (2012)
- 783 55. Perry JL, Reuter KG, Kai MP, Herlihy KP, Jones SW, Luft JC, Napier M, Bear JE, DeSimone
- JM. PEGylated PRINT Nanoparticles: The Impact of PEG Density on Protein Binding,
- Macrophage Association, Biodistribution, and Pharmacokinetics. *Nano Lett* (2012) 12:5304–
- 786 5310. doi: 10.1021/nl302638g
- 787 56. Altintoprak K, Seidenstücker A, Welle A, Eiben S, Atanasova P, Stitz N, Plettl A, Bill J,
- Gliemann H, Jeske H, et al. Peptide-equipped tobacco mosaic virus templates for selective and
- 789 controllable biomineral deposition. *Beilstein Journal of Nanotechnology* (2015) 6:1399–1412.
- 790 doi: 10.3762/bjnano.6.145
- 791 57. Pitek AS, Wen AM, Shukla S, Steinmetz NF. The Protein Corona of Plant Virus Nanoparticles
- Influences their Dispersion Properties, Cellular Interactions, and In Vivo Fates. *Small* (2016)
- 793 12:1758–1769. doi: 10.1002/smll.201502458

- 794 58. Pamujula S, Hazari S, Bolden G, Graves RA, Chinta DD, Dash S, Kishore V, Mandal TK.
 795 Cellular delivery of PEGylated PLGA nanoparticles. *Journal of Pharmacy and Pharmacology*
- 796 (2011) 64:61–67. doi: 10.1111/j.2042-7158.2011.01376.x
- 797 59. Li Y-P, Pei Y-Y, Zhang X-Y, Gu Z-H, Zhou Z-H, Yuan W-F, Zhou J-J, Zhu J-H, Gao X-J.
- 798 PEGylated PLGA nanoparticles as protein carriers: synthesis, preparation and biodistribution
- 799 in rats. Journal of Controlled Release (2001) 71:203–211. doi: 10.1016/S0168-
- 800 3659(01)00218-8
- 801 60. Rabanel J-M, Hildgen P, Banquy X. Assessment of PEG on polymeric particles surface, a key
- step in drug carrier translation. *Journal of Controlled Release* (2014) 185:71–87. doi:
- 803 10.1016/j.jconrel.2014.04.017
- 804 61. O'Riordan CR, Lachapelle A, Delgado C, Parkes V, Wadsworth SC, Smith AE, Francis GE.
- PEGylation of Adenovirus with Retention of Infectivity and Protection from Neutralizing
- 806 Antibody in Vitro and in Vivo. *Hum Gene Ther* (1999) 10:1349–1358. doi:
- 807 10.1089/10430349950018021
- 808 62. Armstrong JK, Hempel G, Koling S, Chan LS, Fisher T, Meiselman HJ, Garratty G. Antibody
- against poly(ethylene glycol) adversely affects PEG-asparaginase therapy in acute
- lymphoblastic leukemia patients. *Cancer* (2007) 110:103–111. doi: 10.1002/cncr.22739
- 811 63. García-Álvarez R, Vallet-Regí M. Hard and Soft Protein Corona of Nanomaterials: Analysis
- and Relevance. *Nanomaterials (Basel)* (2021) 11: doi: 10.3390/nano11040888
- 813 64. Blume JE, Manning WC, Troiano G, Hornburg D, Figa M, Hesterberg L, Platt TL, Zhao X,
- Cuaresma RA, Everley PA, et al. Rapid, deep and precise profiling of the plasma proteome
- with multi-nanoparticle protein corona. *Nat Commun* (2020) 11:3662. doi: 10.1038/s41467-
- 816 020-17033-7

- 817 65. Szekeres GP, Fernández-Iglesias N, Kneipp J, Montes-Bayón M, Bettmer J. Mass
- spectrometric approach for the analysis of the hard protein corona of nanoparticles in living
- 819 cells. *J Proteomics* (2020) 212:103582. doi: 10.1016/j.jprot.2019.103582
- 820 66. Steinmetz NF, Manchester M. PEGylated Viral Nanoparticles for Biomedicine: The Impact of
- PEG Chain Length on VNP Cell Interactions In Vitro and Ex Vivo. *Biomacromolecules*
- 822 (2009) 10:784–792. doi: 10.1021/bm8012742